

Interfacial polarization and pyroelectricity in antiferrodistortive structures induced by a flexoelectric effect and rotostriction

Anna N. Morozovska,^{1,2,*} Eugene A. Eliseev,¹ Maya D. Glinchuk,¹ Long-Qing Chen,³ and Venkatraman Gopalan^{3,†}

¹*Institute for Problems of Materials Science, National Academy of Science of Ukraine, 3, Krjijanovskogo, 03142 Kiev, Ukraine*

²*Institute of Semiconductor Physics, National Academy of Science of Ukraine, 41, pr. Nauki, 03028 Kiev, Ukraine*

³*Department of Materials Science and Engineering, Pennsylvania State University, University Park, Pennsylvania 16802, USA*

(Received 23 October 2011; revised manuscript received 6 January 2012; published 21 March 2012)

Theoretical analysis based on the Landau-Ginzburg-Devonshire theory is used to show that the combined effect of flexoelectricity and rotostriction can lead to a spontaneous polarization and pyroelectricity in the vicinity of antiphase boundaries, structural twin walls, surfaces, and interfaces in the octahedrally tilted phase of otherwise nonferroelectric perovskites such as CaTiO_3 , SrTiO_3 , and EuTiO_3 . As an example, we numerically demonstrate a spontaneous polarization and pyroelectric response at the SrTiO_3 antiphase and twin boundaries at temperatures lower than the antiferrodistortive structural phase transition temperature of $T_S \sim 105$ K in agreement with previously unexplained experimental results. At temperatures lower than effective Curie temperature T_C^* (~ 25 K for twins and ~ 50 K for antiphase boundaries) biquadratic coupling between oxygen octahedron tilt and polarization vectors essentially enhances the polarization induced by the combined flexoelectric and rotostriction effects near the hard domain wall. Biquadratic coupling cannot induce polarization inside easy twins and antiphase boundaries; their polarization and pyroelectricity originates below T_S from the built-in flexoelectric field. The spontaneous polarization reaches the values ~ 0.1 – $5 \mu\text{C}/\text{cm}^2$ at the SrTiO_3 antiphase boundaries and twins without free charges. A principal difference between the influence of biquadratic and flexoelectric couplings on the interfacial polarization is the following: the biquadratic coupling induces bistable ferroelectric polarization inside hard antiphase boundaries and hard twins below T_C^* , while the flexoelectric coupling induces improper spontaneous polarization via the flexoelectric field below T_S .

DOI: [10.1103/PhysRevB.85.094107](https://doi.org/10.1103/PhysRevB.85.094107)

PACS number(s): 77.80.Dj, 68.35.-p, 77.84.Cg, 81.30.-t

I. INTRODUCTION

Unique multifunctional properties of oxide interfaces are currently of widespread interest. These include two-dimensional electron gas, superconductivity,^{1–3} charged domain walls,⁴ magnetism,^{5,6} and multiferrocity at oxide interfaces⁷ and thin strained films.⁸ Interfaces by nature possess gradients of various order parameters such as strain, octahedral rotations, polarization, and magnetization, which can couple to induce new phenomena not present in the relevant bulk materials.⁹ The influence of strain^{8,10} and strain gradients^{11–13} in inducing ferroelectric polarization is well known. Recently, improper ferroelectricity induced by coupling to octahedral rotations has been predicted in a number of oxides [e.g., YMnO_3 ,¹⁴ $\text{Ca}_3\text{Mn}_2\text{O}_7$,¹⁵ CaTiO_3 (Ref. 16)] and their multilayers.¹⁷

Interfaces in antiferrodistorted perovskite oxides can possess both gradients in strain u_{ij} and in oxygen octahedral rotations, characterized by spontaneous octahedral tilt angles, which in turn can be described by an axial vector Φ_i ($i = 1, 2, 3$).¹⁸ As a consequence, both direct flexoelectric effect, namely, the creation of a ferroelectric polarization due to a strain gradient, as well as rotostriction, namely, a quadratic coupling between octahedral rotations and strain, exist at such interfaces. The coupling between these two phenomena can thus lead to a ferroelectric polarization at an interface across which the octahedral rotation varies, which is the subject of this paper. It has been previously predicted that a spontaneous polarization vector P_i can appear inside structural walls due to biquadratic coupling term $\eta_{ijkl} P_i P_j \Phi_k \Phi_l$,^{19,20} but it is absent in the bulk. The biquadratic coupling term was

later regarded as Houchmandazeh-Laizerowicz-Salje (HLS) coupling.²¹ The coupling was considered as the reason for magnetization appearance inside the ferromagnetic domain wall in nonferromagnetic media.²² Biquadratic coupling leads to a polarization appearance inside antiphase boundaries in SrTiO_3 below 50 K.²⁰ Zubko *et al.*²³ experimentally observed strong changes of the apparent flexoelectric coefficient in SrTiO_3 at much higher temperatures, namely, below the antiferrodistortive structural phase transition temperature (105 K), and supposed one of its possible reasons in the polarization appearance at the domain walls between twins. Recently Salje *et al.* directly observed ferroelectric polarization at ferroelastic domain boundaries in CaTiO_3 by aberration-corrected transmission electron microscopy (TEM) at room temperature.²⁴

To the best of our knowledge, the flexoelectricity-induced polarization appearance across the structural twin boundaries (TB), antiphase boundaries (APBs), and interfaces has not been previously addressed. However, the flexoelectric coupling, which is nonzero in any material and strong enough in many perovskites,^{11,13,23,25–28} should lead to the spontaneous polarization appearance across the structural domain walls of otherwise nonferroelectric perovskites. Direct gradient coupling between the order parameters could lead to the oscillatory solutions and nonuniform pattern formation.^{29,30} This motivates us to perform calculations, based on the Landau-Ginzburg-Devonshire (LGD) free energy, to study the impact of flexoelectric coupling on the spontaneous polarization in the vicinity of structural domain walls in nonferroelectric tilted perovskites such as SrTiO_3 , CaTiO_3 , and EuTiO_3 . We present results for 90° TB and 180° APBs in bulk SrTiO_3 .

II. THEORETICAL FORMALISM

Following Tagantsev *et al.*,²⁰ we analyze the domain-wall energy using an approximate free-energy functional corresponding to Taylor expansion on the polar and structural order-parameter components. In the parent high-temperature phase above the structural phase transition, the free-energy density has the form

$$\begin{aligned}
 F_b = & a_i(T)P_i^2 + a_{ij}''P_i^2P_j^2 + \dots + \frac{g_{ijkl}}{2} \left(\frac{\partial P_i}{\partial x_j} \frac{\partial P_k}{\partial x_l} \right) \\
 & - P_i \left(\frac{E_i^d}{2} + E_i^{\text{ext}} \right) - q_{ijkl}u_{ij}P_kP_l + \frac{c_{ijkl}}{2}u_{ij}u_{kl} \\
 & + b_i(T)\Phi_i^2 + b_{ij}''\Phi_i^2\Phi_j^2 - \eta_{ijkl}''P_iP_j\Phi_k\Phi_l \\
 & + \frac{v_{ijkl}}{2} \left(\frac{\partial \Phi_i}{\partial x_j} \frac{\partial \Phi_k}{\partial x_l} \right) - r_{ijkl}^{(\Phi)}u_{ij}\Phi_k\Phi_l \\
 & + \frac{f_{ijkl}}{2} \left(\frac{\partial P_k}{\partial x_l} u_{ij} - P_k \frac{\partial u_{ij}}{\partial x_l} \right) - \Phi_i\tau_i^d. \quad (1)
 \end{aligned}$$

Φ_i is the components ($i = 1, 2, 3$) of an axial tilt vector corresponding to the octahedral rotation angles¹⁸ (see Fig. 1), τ_i^d is deelasitication torque,¹⁸ and $u_{ij}(\mathbf{x})$ is the strain tensor. The summation is performed over all repeated indices. Coefficients $a_i(T)$ and $b_i(T)$ temperature dependence can be fitted with Barrett law for quantum paraelectrics:³¹ $a_1(T) = \alpha_T T_q^{(E)} [\coth(T_q^{(E)}/T) - \coth(T_q^{(E)}/T_0^{(E)})]$ and $b_1(T) = \beta_T T_q^{(\Phi)} [\coth(T_q^{(\Phi)}/T) - \coth(T_q^{(\Phi)}/T_S)]$. Gradient coefficients g_{ij} and v_{ij} are regarded positive for commensurate ferroics. f_{ijkl} is the fourth-rank tensor of flexoelectric coupling, q_{ijkl} is the fourth-rank electrostriction tensor, $r_{ijkl}^{(\Phi)}$ is the rotostriction tensor. The biquadratic coupling between Φ_i and polarization components P_i is defined by the constants η_{ijkl} . The flexoelectric effect tensor f_{ijkl} and rotostriction tensor $r_{ijkl}^{(\Phi)}$ have nonzero components in all phases and for any symmetry of the system. Tensor form for cubic $m3m$ symmetry is well known; in particular, f_{12} , f_{11} , and f_{44} are nonzero,²³ similarly to elastic constants and electrostriction tensors.³² Note, that the inclusion of the flexoelectric Lifshitz term in the free energy is critical for all effects discussed below.

External field is E_i^{ext} . In a general case polarization distribution $P_i(x_i)$ can induce the depolarization field E_i^d inside

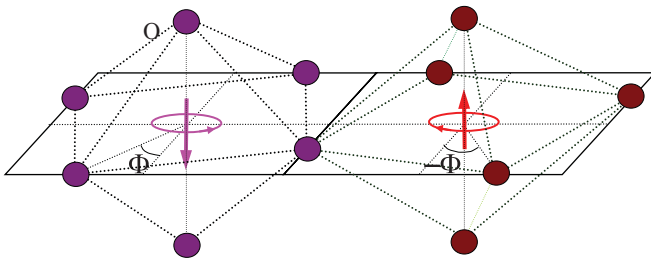


FIG. 1. (Color online) The tilt value is typically opposite for the neighboring oxygen octahedra far from the domain boundaries.¹⁸ For the case free energy (1) considers the quasicontinuum tilt behavior in the next-nearest octahedral.^{20,30}

the wall. In the dielectric limit E_i^d obeys electrostatic equation

$$\varepsilon_0 \varepsilon_b \frac{\partial E_i^d}{\partial x_i} = - \frac{\partial P_i}{\partial x_i} \quad (i = 1, 2, 3), \quad (2)$$

where $\varepsilon_0 = 8.85 \times 10^{-12}$ F/m is the universal dielectric constant, ε_b is the “base” isotropic lattice permittivity, different from the ferroelectric soft-mode permittivity.^{33–36} A semiconductor case is considered elsewhere.³⁷

Euler-Lagrange equations of state are obtained from the minimization of the free energy (1) as

$$\frac{\partial F_b}{\partial \Phi_i} - \frac{\partial}{\partial x_j} \left(\frac{\partial F_b}{\partial (\partial \Phi_i / \partial x_j)} \right) = 0, \quad (3a)$$

$$\frac{\partial F_b}{\partial P_i} - \frac{\partial}{\partial x_j} \left(\frac{\partial F_b}{\partial (\partial P_i / \partial x_j)} \right) = 0, \quad (3b)$$

$$\frac{\partial F_b}{\partial u_{ij}} - \frac{\partial}{\partial x_k} \left(\frac{\partial F_b}{\partial (\partial u_{ij} / \partial x_k)} \right) = \sigma_{ij}, \quad (3c)$$

where $\sigma_{ij}(\mathbf{x})$ is the stress tensor that satisfies mechanical equilibrium equation $\partial \sigma_{ij}(\mathbf{x}) / \partial x_j = 0$. Note, that the stress tensor, polarization, and tilt gradients vanish far from the domain walls.

Equations of state (3c) could be rewritten via the strains $u_{ij}(\mathbf{x})$ as follows:

$$u_{mn} = s_{mnij}\sigma_{ij} + R_{mnl}^{(\Phi)}\Phi_k\Phi_l + Q_{mnl}P_kP_l - F_{mnl}\frac{\partial P_k}{\partial x_l}, \quad (4)$$

where s_{mnij} is the elastic compliances tensor, $R_{ijkl}^{(\Phi)} = s_{ijmn}r_{mnl}^{(\Phi)}$ is the rotostriction strain tensor, $Q_{ijkl} = s_{ijmn}q_{mnl}$ is the electrostriction strain tensor, and $F_{ijkl} = s_{ijmn}f_{mnl}$ is the flexoelectric strain tensor. The latter term corresponds to inverse flexoelectric effect.

The inhomogeneous strain $u_{ij}(\mathbf{x})$ given by Eq. (4) induces the polarization variation $\delta P_i(\mathbf{x})$ across the structural APBs and TBs, domain walls, defects, and interfaces due to the direct flexoelectric effect:

$$\delta P_i(\mathbf{x}) \sim a_{iv}^{-1} f_{mnl} \frac{\partial u_{mn}}{\partial x_l} \sim -a_{iv}^{-1} f_{mnl} R_{mnpq}^{(\Phi)} \frac{\partial (\Phi_p \Phi_q)}{\partial x_l}. \quad (5)$$

The term $f_{mnl} \frac{\partial u_{mn}}{\partial x_l}$ denotes direct flexoelectric effect. Note, that Eq. (5) is valid only for zero electric field, including both external and depolarization fields. The proportionality in Eq. (5) suggests that the product of the flexoelectric f_{mnl} and rotostriction $R_{mnpq}^{(\Phi)}$ coefficients leads to the appearance of spontaneous polarization, which will be abbreviated in this study as flexo-roto-effect. To the best of our knowledge, the flexoelectric contribution to the interfacial polarization has not been considered earlier.

The gradient in the octahedral tilts across APBs or TBs may lead to a rather strong interfacial polarization due to the derivatives of the rotation angle in Eq. (5). In the next section we will consider the concrete example of SrTiO₃ with known numerical values of $R_{mnl}^{(\Phi)}$ and F_{mnl} to check the validity of this supposition.

III. FLEXO-ROTO-EFFECT CONTRIBUTION TO THE INTERFACIAL POLARIZATION AND PYROELECTRICITY

Below we consider several one-dimensional problems, which follow from general results of the previous section, namely, a typical 180° APB and 90° TB. Stable solutions of the coupled Euler-Lagrange equations (3) were obtained numerically by iteration method. We set initial distributions of the tilt and polarization vectors, which satisfy the boundary conditions. Special attention was paid to the parity of the obtained polarization distributions, namely, we consider both odd and even initial polarization distributions with respect to the domain-wall plane. Iterations were stopped when the relative tolerance reached the value 10^{-4} .

Note that Tagantsev *et al.*²⁰ obtained nonzero polarization across APBs in SrTiO₃ below $T_C^* \sim 40$ K, where T_C^* is a local ferroelectric transition temperature in APBs in a free crystal. The flexoelectric coupling was not included into the calculations performed in Ref. 20, while mentioned in the paper as giving rise to the renormalization of the gradient terms. One of the most important results we obtained in the present research is the fact that the flexoelectric effect primary leads to the appearance of the strong built-in electric fields across the wall, besides the renormalization of the polarization gradient term also considered in Ref. 27. We obtained that the flexoelectric effect can induce the polarization and pyroelectric response across TB and APB walls over the entire temperature range of the structural phase $T_S < 105$ K.

Despite odd distributions seeming to be more energetically preferable,³⁷ one may question the experimental observation of odd polarization and pyroelectric response distributions across an interface, because the mean values are zero in this case. Using aberration-corrected TEM combined with atomic column shape image analysis (proposed earlier in Ref. 38) it is possible to achieve picometer resolution (0.025 nm for atomic coordinates) and to observe spontaneous polarization at ferroelastic domain twin boundaries.²⁴ To the best of our understanding, Figs. 2(e) and 2(f) in Ref. 24 reliably demonstrate signatures of both even and odd polarization distributions across ferroelastic twins in CaTiO₃. So we hope that local spontaneous polarization of elastic domain walls in ferroelastics such as CaTiO₃, SrTiO₃, and EuTiO₃ can be reliably observed by aberration-corrected TEM.

Below we show that all ferroelastic domain walls possess noticeable pyroelectric coefficients that can be of odd and even type with respect to the domain-wall plane. Spatial distribution of pyroelectric coefficients (regarded as local pyroelectric response) can be directly measured by novel scanning probe pyroelectric microscopy (PyroSPM), where the resolution limit 50 nm was already achieved.³⁹ Similar to the conventional piezoelectric force microscopy, where the lateral resolution is at least 2–5 times smaller than the tip effective size (see, e.g., Fig. 12 in Ref. 40), the resolution in PyroSPM is primarily determined by the sharpness of the tip. So, scanning with tips of sizes 5–10 nm (Ref. 41) allow registration of local piezoresponse and with lateral resolution ~ 2 –5 nm (see, e.g., Refs. 41 and 42, and references therein) and potentially local pyroelectric response with the same resolution. Since half width of “hard” APBs and TBs in SrTiO₃ is about 3–5 nm,^{20,37}

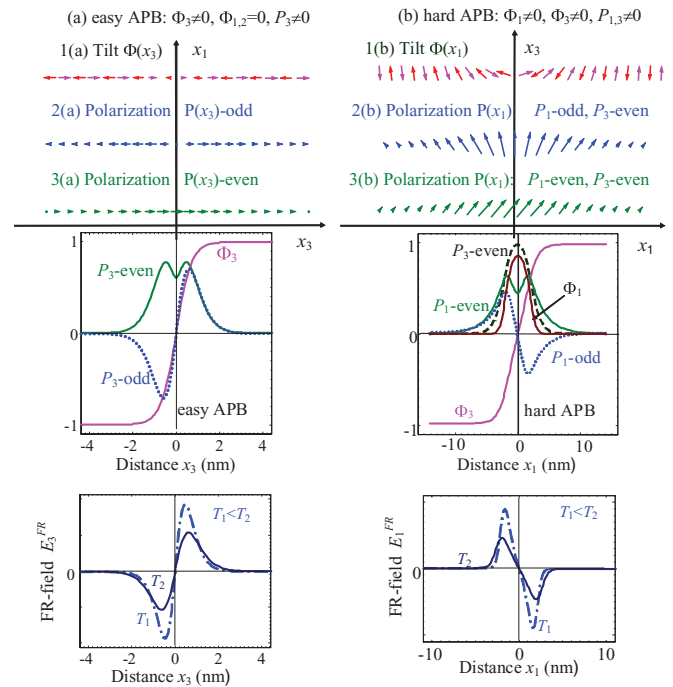


FIG. 2. (Color online) Schematics of the polarization appearance inside easy (a) and hard (b) APBs. $x_1 = [100]$, $x_3 = [001]$, and $x_2 = [010]$ (not shown), are crystallographic axes directions of SrTiO₃. Flexo-rotto field, which induces the polarization component parallel to the wall, is shown at the bottom plots at two different temperatures $T_1 < T_2$. Note that Vasudevarao *et al.*⁸ observed and calculated by phase-field various orientations of the ferroelastic APB in SrTiO₃.

PyroSPM could reliably detect pyroelectric response averaged over the wall width. Thus below we consider the influence of the flexoelectric and rotostriction effect on both odd and even polarization distributions across TBs and APBs. Also we calculate the maximal values of pyroelectric coefficients as well as average the values over the domain-wall width.

A. Flexo-rotto-effect manifestation at the APB

In the octahedral tilted phase at $T < T_S$, the one-component spontaneous tilt Φ_3^S appears in bulk SrTiO₃; other components, Φ_1 and Φ_2 , can be nonzero in the vicinity of APBs. “Easy” APBs with $\Phi_3(x_3) \neq 0, \Phi_2 \equiv 0, \Phi_1 \equiv 0$ [see Fig. 2(a)] induces nonzero odd or even distribution of polarization $P_3(x_3)$, while $P_1 \equiv 0$ and $P_2 \equiv 0$. “Hard” APBs with $\Phi_1(x_1) \neq 0, \Phi_3(x_1) \neq 0, \Phi_2 \equiv 0$ [see Fig. 2(b)] induces nonzero odd or even distributions of polarization $P_1(x_1)$ and even distribution of $P_3(x_1)$, while $P_2 \equiv 0$. The classifications “easy” and “hard” APB come from Ref. 20.

For the case of hard APBs (x_1 -dependent solution) we derive the stress field and simplify the evident form of Eqs. (3) as listed in section S1 of the Supplemental Material.⁴³ Distributions $\Phi_{1,3}(x_3)$ and $P_{1,3}(x_3)$ are shown schematically in Fig. 2(b) (right). It appears that $\Phi_{1,3}(x_3)$ are rather weakly dependent on the polarization vector. Nonzero odd electric field $E_1^{FR} = -F_{12}(s_{11} + s_{12})^{-1} \partial [(R_{11}^{(\Phi)} + R_{12}^{(\Phi)}) \Phi_3^2 + 2R_{12}^{(\Phi)} \Phi_1^2] / \partial x_1$ induced by flexoelectric effect and rotostriction (abbreviated as flexo-rotto field

below) exists only for the polarization component $P_1(x_1)$ perpendicular to the APB plane [see bottom Fig. 2(b)]. It is clear that the odd field makes odd-type distribution of $P_1(x_1)$ favorable. The component P_1 appears just below T_S and strongly depends on the tilt vector as proportional to the field E_1^{FR} . Hysteresis loop for polarization component P_1 is absent in external field E_1^{ext} due to the strong depolarization field $E_1^d(x_1) = -P_1(x_1)/(\epsilon_0\epsilon_b)$. Nonzero component P_1 perpendicular to the APB should induce the component P_3 parallel to the APB just below T_S due to the biquadratic coupling term $-\eta_{44}\Phi_1\Phi_3P_1$. Thus the trivial solution $P_1 \equiv P_3 \equiv 0$ does not exist in the vicinity of hard APBs due to nonzero odd $E_1^{FR} \neq 0$ and the coupling term $-\eta_{44}\Phi_1\Phi_3P_1$ (compare with Ref. 20, where the stability of the trivial solution $P_3 \equiv 0$ was studied without flexo-effect). The effective Curie temperature $T_C^{\text{APB}} \approx 50$ K can be introduced for hard APBs. Ferroelectric hysteresis for polarization component $P_3(E_3^{\text{ext}})$ should exist in the temperature range $T < T_C^{\text{APB}}$. Below T_C^{APB} the perpendicular component P_1 is induced by the sum of the coupling term $-\eta_{44}\Phi_1\Phi_3P_3$ and flexoroto field E_3^{FR} . The depolarization field strongly reduces the component P_1 in comparison with ferroelectric polarization P_3 below T_C^{APB} . Pyroelectric coefficients $\Pi_3 = dP_3/dT$ and $\Pi_1 = dP_1/dT$ are nonzero in the temperature range $T < T_S$, but their temperature behavior is rather different at $T_C^{\text{APB}} < T < T_S$ and $T < T_C^{\text{APB}}$, as shown in Fig. 3.

Under the absence of the flexoelectric field the spontaneous polarization and pyroelectric coefficient are zero at temperatures higher than the effective Curie temperature T_C^{APB} (see curves 1 and 2 calculated at $F_{ij} \equiv 0$ and $\eta_{ij} \neq 0$ in Fig. 3). The flexoelectric field rather weakly influences the polarization component P_3 [compare curves 1 and 2 with curves 3 and 4 in Fig. 3(a)]. However, the flexoelectric field E_1^{FR} strongly increases the component P_1 below T_S , since $P_1 \sim E_1^{FR}$ [compare curves 1 and 2 with curves 3 and 4 in Fig. 3(b)]. Actually, for the case $F_{ij} \neq 0$ the component P_1 appears below T_S , first quasilinearly increases with temperature decrease, then has a pronounced jump at T_C^{APB} , and then saturates at temperatures $T \ll T_q$. The break at T_C^{APB} originates from the appearance of reversible polarization component P_3 below T_C^{APB} . The component $P_1 \sim E_1^{FR} \sim \frac{\partial \Phi^2}{\partial x_1} \sim (\Phi_3^S)^2/l_\Phi \sim [-b_1(T)]^{3/2} \sim (T_S - T)^{3/2}$ in the vicinity of T_S , where $l_\Phi = \sqrt{-v_{11}/b_1(T)}$ is the correlation length. Note that Tagantsev *et al.*²⁰ analytically predicted spontaneous polarization about $4 \mu\text{C}/\text{cm}^2$ at hard APBs below 35–40 K without considering flexo-roto-effect contribution. Allowing for the flexo-roto-effect we obtained $P_3 \sim 8 \mu\text{C}/\text{cm}^2$ and $P_1 \sim 0.1 \mu\text{C}/\text{cm}^2$ at hard APBs below $T_C^{\text{APB}} \approx 50$ K. At temperatures $T < T_C^{\text{APB}}$ the amplitude of P_1 is much smaller than the amplitude of P_3 due to the strong depolarization field $E_1^d(x_1)$.

It is seen from Figs. 3(c) and 3(d) that pyroelectric coefficients Π_3 and Π_1 appear below $T_S = 105$ K only at nonzero flexoelectric coefficient $F_{12} \neq 0$. Pyroelectric coefficient Π_3 has the sharp maximum at T_C^{APB} corresponding to the second-order ferroelectric phase transition (appearance of the ferroelectric polarization P_3). Pyroelectric coefficient Π_1 has two maximums: a smooth maximum at the polarization inflection point ~ 80 K and the sharp maximum at T_C^{APB} originated from P_3 appearance, since P_3 enhances P_1 via

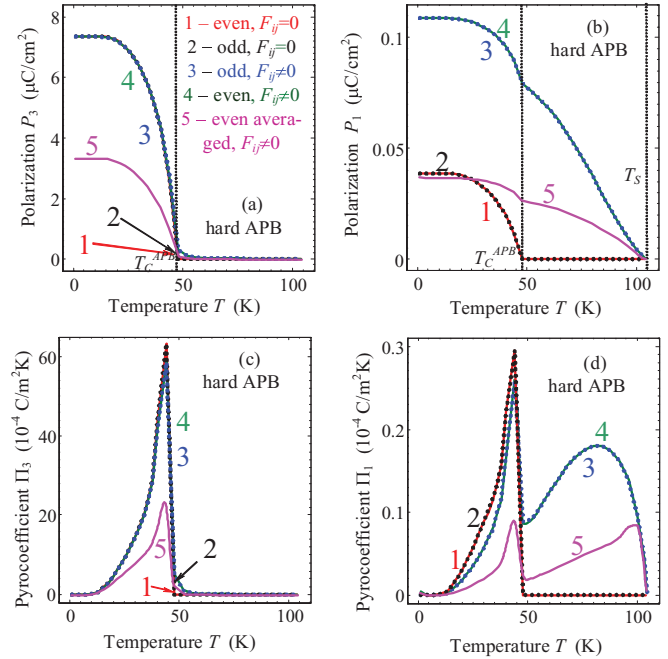


FIG. 3. (Color online) Temperature dependences of spontaneous polarization components P_3 and P_1 [(a), (b)] and corresponding pyroelectric coefficient components Π_3 and Π_1 values [(c), (d)] calculated for hard APBs in SrTiO_3 without free screening charges. Temperature dependences are calculated for nonzero flexoelectric effect $F_{ij} \neq 0$ and biquadratic coupling $\eta_{ij} \neq 0$ (curves 3,4,5) and for the case of nonzero biquadratic coupling $\eta_{ij} \neq 0$ and zero flexoelectric effect $F_{ij} \equiv 0$ (curves 1,2). Curves 1–4 are maximal values, curves 5 are the even-type distributions averaged across APB width, for which temperature dependence is shown in Fig. S2, Supplemental Material (Ref. 43). Curves 1–5 style and color coding for plots (a)–(d) are the same and described in the legend to plot (a). Solid and dotted curves correspond to P_3 -even and P_3 -odd solutions, respectively. Material parameters are listed in the Table I.

the biquadratic coupling term $-\eta_{44}\Phi_1\Phi_3P_3$. Pyroelectric coefficients monotonically decrease below T_C^{APB} with the temperatures decreasing due to the spontaneous polarization component saturation at temperatures $T \ll T_q$. Actually, in the range $T \ll T_q$ polarization becomes almost temperature independent and its temperature derivative vanishes.

Allowing for the flexo-roto-effect contribution we calculated noticeable pyroelectric coefficients of the even-type distributions averaged across hard APBs: $\langle \Pi_3 \rangle \sim 2 \times 10^{-3} \text{ C}/\text{m}^2 \text{ K}$ around T_C^{APB} and $\langle \Pi_1 \rangle \sim 1 \times 10^{-5} \text{ C}/\text{m}^2 \text{ K}$. The values are well above detectable limits of pyroelectric coefficients, which are about $(10^{-6} - 10^{-7}) \text{ C}/\text{m}^2 \text{ K}$.⁴⁴ The half-width of hard APBs is not less than 3 nm at 0 K and 5 nm at 90 K (see Fig. S2, Supplemental Material⁴³). Thus PyroSPM³⁹ supplied with sharp tips of sizes 5–10 nm could reliably detect pyroelectric response averaged over the APB widths.

For the case of easy APBs (x_3 -dependent solution) one could easily derive the stress field and the evident form of Eqs. (3) as listed in section S2 of the Supplemental Material.⁴³ Distributions of $\Phi_3(x_3)$ and $P_3(x_3)$ are shown schematically in Fig. 2(a) (right). The tilt $\Phi_3(x_3)$ profile is rather weakly dependent on the polarization vector distribution and could be well approximated as $\Phi_3 = \Phi_3^S \tanh(x_3/\sqrt{2}l_\Phi)$.

TABLE I. SrTiO₃ material parameters and LGD free energy (1) coefficients collected from Refs. 20, 23, 31, and 45–49. Superscripts “u” and “s” denote coefficients at given strain (clamped sample) and given stress (free sample), respectively.

Parameter	SI units	Value	Source and notes
ε_b	Dimensionless	43	48
α_T	$10^6 \times \text{m}/(\text{F K})$	0.75	20,46
$T_0^{(E)}$	K	30	<i>ibid.</i>
$T_q^{(E)}$	K	54	<i>ibid.</i>
a_{ij}	$10^9 \times \text{m}^5/(\text{C}^2\text{F})$	$a_{11}^u = 2.025, a_{12}^u = 1.215,$ $a_{11}^s = 0.820, a_{12}^s = 1.396$	<i>ibid.</i>
q_{ij}	$10^{10} \times \text{m}/\text{F}$	$q_{11} = 1.251, q_{12} = -0.108,$ $q_{44} = 0.243$	46
Q_{ijkl}	m^4/C^2	$Q_{11} = 0.051, Q_{12} = -0.016,$ $Q_{44} = 0.020$	20
g_{ijkl}	$10^{-11} \times \text{V m}^3/\text{C}$	$g_{11} = g_{44} = 1, g_{12} = 0.5$	Estimation (Ref. 49)
β_T	$10^{26} \times \text{J}/(\text{m}^5 \text{K})$	9.1	46
T_S	K	105	46
$T_q^{(\Phi)}$	K	145	46
b_{ij}	$10^{50} \times \text{J}/\text{m}^7$	$b_{11}^u = 1.94, b_{12}^u = 3.96,$ $b_{11}^s = 0.93, b_{12}^s = 3.88$	46
r_{ij}	$10^{30} \times \text{J}/(\text{m}^5)$	$r_{11} = 1.3, r_{12} = -2.5,$ $r_{44} = -2.3$	46
R_{ij}	$10^{19} \times \text{m}^{-2}$	$R_{11} = 0.882, R_{12} = -0.777,$ $R_{44} = -1.811$	Calculated from r_{ij}
η_{ijkl}	$10^{29} (\text{F m})^{-1}$	$\eta_{11}^u = -3.366, \eta_{12}^u = 0.135, \eta_{44}^u = 6.3$ $\eta_{11}^s = -2.095, \eta_{12}^s = -0.849,$ $\eta_{44}^s = 5.860$	46 Calculated from η_{ij}^u
v_{ijkl}	$10^{10} \times \text{J}/\text{m}^3$	$v_{11} = 0.28, v_{12} = -7.34,$ $v_{44} = 7.11$	20
c_{ij}	$10^{11} \times \text{J}/\text{m}^3$	$c_{11} = 3.36, c_{12} = 1.07,$ $c_{44} = 1.27$	20,46
s_{ij}	$10^{-12} \times \text{m}^3/\text{J}$	$s_{11} = 3.52, s_{12} = -0.85,$ $s_{44} = 7.87$	Calculated from c_{ij}
F_{ijkl}	$10^{-12} \times \text{m}^3/\text{C}$	$F_{11} = -13.80, F_{12} = 6.66,$ $F_{44} = 8.48$	Calculated from f_{ij} from 23 at given stress
Φ_S	Radian	0.0235	At low temperatures

In contrast, polarization P_3 strongly depends on the tilt vector as proportional to the odd flexo-roto field $E_3^{FR} = -2F_{12}R_{12}^{(\Phi)}(s_{11} + s_{12})^{-1}\partial(\Phi_3^2)/\partial x_3$ [see bottom Fig. 2(a)]. The trivial solution $P_3 \equiv 0$ does not exist in the vicinity of APBs due to nonzero flexo-roto field $E_3^{FR} \neq 0$. So the spontaneous polarization component P_3 perpendicular to the APB plane is induced by the flexo-roto-field E_3^{FR} only. The depolarization field $E_3^d(x_3) = -P_3(x_3)/(\varepsilon_0\varepsilon_b)$ (Ref. 52) strongly reduces P_3 value. The “true” ferroelectricity (i.e., polarization hysteresis is absent in external field E_3^{ext} , but nonzero pyroelectric response $\Pi_3 = dP_3/dT$) should exist, since the polarization component is temperature dependent.³⁷ We omit quantitative analyses of the results for the easy APBs in SrTiO₃, because their half-width $\sim l_\Phi(T) = \sqrt{-v_{11}/b_1(T)}$ appeared not more than 1 nm for temperatures less than 90 K (see Fig. S2 in the Supplemental Material⁴³), and sometimes the distance between polarization maxima and minima is less than the unit cell at $T < 90$ K. The features scale less than 1 nm is well beyond applicability of the continuous medium theory we used in the paper.

B. Flexo-roto-effect manifestation at 90° TB

90° twins can have structure with rotation vector parallel [Fig. 4(a)] or perpendicular [Fig. 4(b)] to the domain-wall plane in the immediate vicinity of the plane. Far from the wall the tilt vectors of twins are perpendicular. We will regard parallel twins as hard TB, since they have higher energy, and perpendicular twins as easy TB, since they have lower energy as demonstrated in section S4 of the Supplemental Material.⁴³ The evident form of Eqs. (3) for twins are listed in section S3 of the Supplemental Material.⁴³

The flexo-roto field $\tilde{E}_1^{FR}(\tilde{x}_1)$ exists for 90° twins; it is an odd function with more complex structure than the one for APBs [see bottom Figs. 4(a) and 4(b) and compare them with the bottom Figs. 2(a) and 2(b)]. Polarization hysteresis for the $\tilde{P}_1(\tilde{E}_1^{\text{ext}})$ component is absent in the dielectric limit due to the strong depolarization field $\tilde{E}_1^d(\tilde{x}_1) = -\tilde{P}_1(\tilde{x}_1)/(\varepsilon_0\varepsilon_b)$. Nonzero component \tilde{P}_1 perpendicular to the TB induces the component \tilde{P}_2 parallel to the TB just below T_S due to the biquadratic coupling term $-\tilde{\eta}_{66}\tilde{\Phi}_1\tilde{\Phi}_2\tilde{P}_1$. The trivial solution $\tilde{P}_1 \equiv \tilde{P}_2 \equiv 0$ does not exist in the vicinity of hard TB

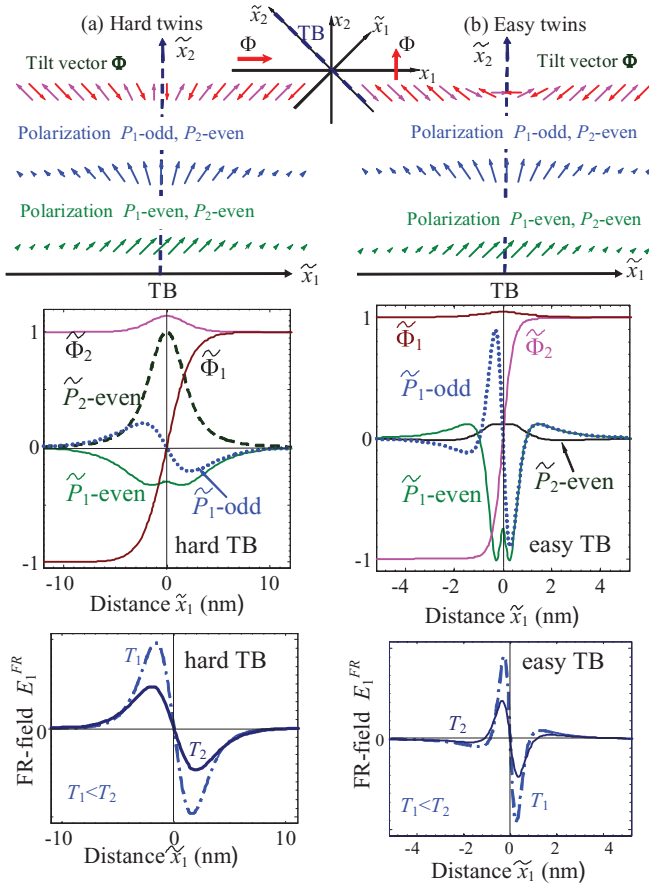


FIG. 4. (Color online) Schematics of 90° TB: rotation vector Φ is parallel (a) or perpendicular (b) to the domain-wall plane in the immediate vicinity of the wall plane. Polarization appears inside the twins. TB plane $\tilde{x} = 0$ (denoted as TB plane) is in the center. Flexo-rotto fields are shown at the bottom plots.

due to nonzero flexo-rotto field $\tilde{E}_1^{FR} \neq 0$ and the coupling term $-\tilde{\eta}_{66}\tilde{\Phi}_1\tilde{\Phi}_2\tilde{P}_1$. Due to the biquadratic coupling terms $-\tilde{\eta}_{11}\tilde{\Phi}_2^2 - \tilde{\eta}_{12}\tilde{\Phi}_1^2$ and elastic fields polarization component \tilde{P}_2 depends on the tilt vector and becomes ferroelectric at temperatures $T < T_C^{TB}$, where the effective Curie temperature $T_C^{TB} \approx 20$ K exists for hard twins in SrTiO₃. Therefore ferroelectric hysteresis for polarization component $\tilde{P}_2(\tilde{E}_2^{ext})$ should exist in the temperature range $T < T_C^{TB}$. Via the biquadratic coupling term $\tilde{\eta}_{66}\tilde{\Phi}_2\tilde{\Phi}_1\tilde{P}_2$ the ferroelectric parallel component \tilde{P}_2 strongly enhances the perpendicular component $\tilde{P}_1(\tilde{E}_1^{FR}) \sim \tilde{E}_1^{FR}$ below T_C^{TB} . Pyroelectric coefficients $\tilde{\Pi}_2 = d\tilde{P}_2/dT$ and $\tilde{\Pi}_1 = d\tilde{P}_1/dT$ should be nonzero in the temperature range $T < T_S$ as shown below.

Under the absence of the flexo-rotto field \tilde{E}_1^{FR} spontaneous polarization and pyroelectric coefficients are zero inside easy TB. Their spontaneous polarization component appears below $T_S = 105$ K at $F_{12} \neq 0$, then quasilinearly increases with temperature decrease and then saturates at temperatures $T < T_0^{(E)} \sim 30$ K. Actually, $\tilde{P}_1 \sim \tilde{E}_1^{FR} \sim \partial(\Phi_2^2)/\partial\tilde{x}_1 \sim (\Phi_S)^2/l_\Phi \sim [-b_1(T)]^{3/2} \sim (T_S - T)^{3/2}$ at temperatures near T_S . Pyroelectric coefficient $\tilde{\Pi}_3$ appears below $T_S = 105$ K at $F_{12} \neq 0$.³⁷ Below we omit quantitative analyses of the results for the easy TB in SrTiO₃, because their half-width appeared not more than 1 nm for temperatures less than 90 K

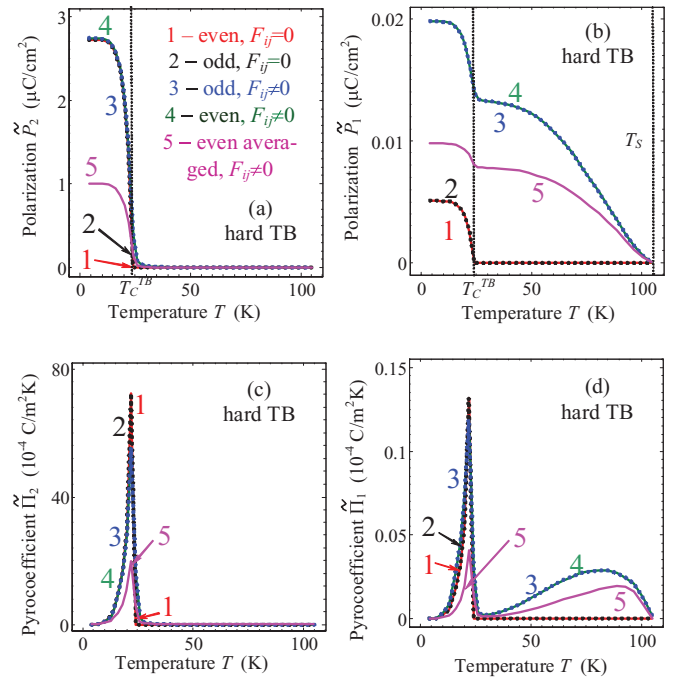


FIG. 5. (Color online) Temperature dependences of spontaneous polarization components \tilde{P}_2 and \tilde{P}_1 maximal values [(a),(b)] and corresponding pyroelectric coefficient components $\tilde{\Pi}_2$ and $\tilde{\Pi}_1$ [(c), (d)] calculated for hard TBs in SrTiO₃ without free carriers. Temperature dependences are calculated for nonzero flexoelectric effect $F_{ij} \neq 0$ and biquadratic coupling $\eta_{ij} \neq 0$ (curves 3,4,5) and for the case of nonzero biquadratic coupling $\eta_{ij} \neq 0$ and zero flexoelectric effect $F_{ij} \equiv 0$ (curves 1,2). Curves 1–4 are maximal values, curves 5 are the even-type distributions averaged across TB width, for which temperature dependence is shown in Fig. S2, Supplemental Material (Ref. 43). Curves 1–5 style and color coding for plots (a)–(d) are the same and described in the legend to plot (a). Material parameters are listed in the Table I.

(see Fig. S2 in Supplemental Material⁴³), and sometimes the distance between polarization maxima and minima is less than the unit cell. As we argued for easy APBs, the features which scale is less than 1 nm cannot be described quantitatively by the continuous medium theory. Note that easy TB half-width noticeably increases with temperature increase only at $T > 90$ K, while polarization amplitude strongly decreases with temperature increases above 90 K and disappears at 105 K.

Polarization and pyroelectric coefficient spatial distribution across hard TB and its temperature behavior are qualitatively similar to the ones calculated for hard APBs. However, numerical values of polarization and pyroelectric coefficients for hard TBs are typically smaller than for hard APBs (compare Fig. 3 with Fig. 5). The difference originated from the smaller effective flexoelectric field, which in turn originated from smaller stress gradients. Differences in the stress gradients originate from the different orientation of the tilt vector Φ inside hard TBs and APBs.

Temperature dependences of the maximal and average spontaneous polarization values calculated inside hard TBs are shown in Figs. 5(a) and 5(b). Under the absence of the flexoelectric field spontaneous polarization and pyroelectric coefficients are zero at temperatures higher than the effective

TABLE II. Interfacial polarization and pyroelectric coefficient properties.

Polarization and pyrocoefficient	Hard 180° tilt APB and hard 90° tilt TB	Easy 180° tilt APB and easy 90° tilt TB
Polarization component P_{\parallel} parallel to the domain wall plane	Ferroelectric hysteresis loop $P_{\parallel}(E_{\parallel})$ exists at $0 < T < T_C^*$ Second-order phase transition to ferroelectric phase occurs at $T = T_C^*$ Hysteresis loop is absent at $T_C^* < T < T_S$. At these temperatures the amplitude P_{\parallel} is proportional to $\eta\Phi_{\perp}\Phi_{\parallel}P_{\perp}$.	Identically zero for easy APB. Negligibly small for easy TB.
Polarization component P_{\perp} perpendicular to the domain wall plane	Amplitude P_{\perp} is proportional to the local flexoelectric field E^{FR} and $\eta\Phi_{\perp}\Phi_{\parallel}P_{\parallel}$ at $0 < T < T_S$. Ferroelectricity and hysteresis loop for $P_{\perp}(E_{\perp})$ is absent due to the strong depolarization field.	Amplitude P_{\perp} is proportional to the local flexoelectric field E^{FR} at $0 < T < T_S$. Ferroelectricity and hysteresis loop for P_{\perp} is absent due to the strong depolarization field.
Pyroelectric response parallel component $\Pi_{\parallel} = dP_{\parallel}/dT$	Increases with T increase at $0 < T < T_C^*$ Sharp maximum occurs at $T = T_C^*$ and then response decreases with T increase at $T_C^* < T < T_S$.	Identically zero for easy APB Negligibly small for easy TB
Pyroelectric response perpendicular component $\Pi_{\perp} = dP_{\perp}/dT$	Increases with T increase at $0 < T < T_C^*$ Sharp maximum occurs at $T = T_C^*$, since in the vicinity of T_C^* $\Pi_{\parallel} \sim \Pi_{\perp}$ via the coupling term $\eta\Phi_{\perp}\Phi_{\parallel}P_{\parallel}$. Smooth maximum exists at polarization inflection point located in the range $T_C^* < T < T_S$.	Π_{\perp} is nonzero in the temperature range $0 < T < T_S$, but vanishes at low temperatures $T \rightarrow 0$ and tends to zero at $T \rightarrow T_S$.

T_C^* is the effective Curie temperature that is different for APBs and TBs, namely, $T_C^{\text{APB}} \approx 50$ K for hard APBs and $T_C^{\text{TB}} \approx 25$ K for hard TBs in SrTiO₃; T_S is the temperature of the structural phase transition. FR is the product of flexoelectric and rotostriction coefficients. η is the biquadratic coupling coefficient.

Curie temperature T_C^{TB} (see curves 1, and 2 calculated at $F_{ij} \equiv 0$ and $\eta_{ij} \neq 0$). The flexo-roto-effect rather weakly influences the polarization component \tilde{P}_2 . For the case $F_{ij} \neq 0$ the component $\tilde{P}_1 \sim E_1^{FR}$ appears below T_S , first quasilinearly increases with temperature decrease, then nonlinearly increases, then has a pronounced jump at T_C^{TB} , and then saturates at low temperatures $T \ll T_q$. The jump at T_C^{TB} originates from the appearance of reversible ferroelectric polarization component \tilde{P}_2 below T_C^{TB} . The maximal values of polarization are very close for odd and even types of solutions in the dielectric limit. Allowing for the flexo-roto-effect contribution we obtained $\tilde{P}_2 \sim 2 \mu\text{C}/\text{cm}^2$ and $\tilde{P}_1 \sim 0.02 \mu\text{C}/\text{cm}^2$ below T_C^{TB} . Without the flexo-roto-effect \tilde{P}_2 is still $\sim 2 \mu\text{C}/\text{cm}^2$ at low temperatures, but $\tilde{P}_1 < 0.005 \mu\text{C}/\text{cm}^2$.

Temperature dependences of the maximal and average pyroelectric coefficients $\tilde{\Pi}_2$ and $\tilde{\Pi}_1$ of hard TB are shown in Figs. 5(c) and 5(d). Pyroelectric coefficients appear below T_S only at nonzero flexoelectric coefficient $F_{ij} \neq 0$. Pyroelectric coefficient $\tilde{\Pi}_1$ has two maximums: a smooth maximum at the polarization inflection point ~ 80 K and the sharp maximum at T_C^{TB} originated from \tilde{P}_2 appearance, since \tilde{P}_2 enhances \tilde{P}_1 via the biquadratic coupling term $\tilde{\eta}_{66}\Phi_2\Phi_1\tilde{P}_2$ in the corresponding equation of state. Pyroelectric coefficient $\tilde{\Pi}_2$ has a single sharp maximum at T_C^{TB} corresponding to the second-order ferroelectric phase transition (appearance of the ferroelectric polarization \tilde{P}_2). Pyroelectric coefficients

monotonically decrease below T_C^{TB} with the temperatures decreasing due to the spontaneous polarization component saturation at temperatures $T \ll T_q$.

Allowing for the flexo-roto-effect contribution we calculated pyroelectric coefficients of the even-type distributions averaged across hard TB: $\langle \tilde{\Pi}_2 \rangle \sim 2 \times 10^{-3} \text{ C}/\text{m}^2 \text{ K}$ and $\langle \tilde{\Pi}_1 \rangle \sim 2 \times 10^{-6} \text{ C}/\text{m}^2 \text{ K}$ around T_C^{TB} . The values of $\langle \tilde{\Pi}_2 \rangle$ are well above the detectable limit, and $\langle \tilde{\Pi}_1 \rangle$ is within the limit.⁴⁴ The half-width of hard TB is not less than 3 nm at 0 K and 5 nm at 90 K (see Fig. S2 of the Supplemental Material⁴³). We hope that PyroSPM³⁹ supplied with sharp tips of sizes 5–10 nm could detect pyroelectric response averaged over the TB widths and thus our results could provide motivation to apply this method to the study of SrTiO₃ domain walls.

To summarize Sec. III, let us emphasize that pyroelectric response and polarization across TBs and APBs in SrTiO₃ originate from the flexo-roto-effect in the temperature range $T_C^{\text{APB, TB}} < T < T_S$ and should exist in other ferroelastic incipient ferroelectrics like in CaTiO₃ and EuTiO₃.

IV. SUMMARY

In summary, we report a mechanism, namely, through the coupling of flexoelectric and rotostriction effects, that can give rise to the appearance of a significant improper spontaneous polarization and pyroelectricity across a structural antiphase

boundary and twins, and by extension across interfaces in otherwise nonferroelectric perovskites such as CaTiO_3 , SrTiO_3 , and EuTiO_3 . In SrTiO_3 , we show that this mechanism leads to a spontaneous polarization and pyroelectricity with an onset at a higher temperature than previously predicted through other coupling mechanisms (Table II).

The spontaneous polarization and average pyroelectric coefficient reaches the values $\sim 0.1\text{--}5 \mu\text{C}/\text{cm}^2$ and $\sim 1 \times 10^{-3} \text{ C}/\text{m}^2 \text{ K}$ at the SrTiO_3 antiphase and twin boundaries. Since the induced polarizations and pyroelectric response are well above detectable limits and since this effect is allowed at interfaces in all structures with static rotations, which are

abundant in nature, it allows for an understanding of a large class of polar interfaces in nonpolar materials.

ACKNOWLEDGMENTS

The authors gratefully acknowledge multiple discussions with Daniel Litvin, Behera K. Rakesh, and Sergei V. Kalinin, useful comments and suggestions from Alexander K. Tagantsev, and especially his idea about interfacial pyroelectricity. National Science Foundation (Grants No. DMR-0908718 and No. DMR-0820404) and user agreement with CNMS N UR-08-869 are also acknowledged.

*morozo@i.com.ua

†vxg8@psu.edu

¹A. Ohtomo, D. A. Muller, J. L. Grazul, and H. Y. Hwang, *Nature (London)* **419**, 378 (2002).

²A. Ohtomo and H. Y. Hwang, *Nature (London)* **427**, 423 (2004).

³J. W. Park, D. F. Bogorin, C. Cen, D. A. Felker, Y. Zhang, C. T. Nelson, C. W. Bark, C. M. Folkman, X. Q. Pan, M. S. Rzchowski, J. Levy, and C. B. Eom, *Nature Communications* **1**, 94 (2010).

⁴J. Seidel, L. W. Martin, Q. He, Q. Zhan, Y.-H. Chu, A. Rother, M. E. Hawkrigge, P. Maksymovych, P. Yu, M. Gajek, N. Balke, S. V. Kalinin, S. Gemming, F. Wang, G. Catalan, J. F. Scott, N. A. Spaldin, J. Orenstein, and R. Ramesh, *Nature Mater.* **8**, 229 (2009).

⁵Ying-Hao Chu, Lane W. Martin, Mikel B. Holcomb, Martin Gajek, Shu-Jen Han, Qing He, Nina Balke, Chan-Ho Yang, Donkoun Lee, Wei Hu, Qian Zhan, Pei-Ling Yang, Arantxa Fraile-Rodríguez, Andreas Scholl, Shan X. Wang, and R. Ramesh, *Nature Mater.* **7**, 478 (2008).

⁶S. J. May, P. J. Ryan, J. L. Robertson, J.-W. Kim, T. S. Santos, E. Karapetrova, J. L. Zarestky, X. Zhai, S. G. E. te Velthuis, J. N. Eckstein, S. D. Bader, and A. Bhattacharya, *Nature Mater.* **8**, 892 (2009).

⁷M. Stengel, D. Vanderbilt, and N. A. Spaldin, *Nature Mater.* **8**, 392 (2009).

⁸A. Vasudevarao, A. Kumar, L. Tian, J. H. Haeni, Y. L. Li, C.-J. Eklund, Q. X. Jia, R. Uecker, P. Reiche, K. M. Rabe, L. Q. Chen, D. G. Schlom, and Venkatraman Gopalan, *Phys. Rev. Lett.* **97**, 257602 (2006).

⁹E. A. Eliseev, A. N. Morozovska, M. D. Glinchuk, B. Y. Zaulychny, V. V. Skorokhod, and R. Blinc, *Phys. Rev. B* **82**, 085408 (2010).

¹⁰D. A. Tenne, A. Bruchhausen, N. D. Lanzillotti-Kimura, A. Fainstein, R. S. Katiyar, A. Cantarero, A. Soukiassian, V. Vaithyanathan, J. H. Haeni, W. Tian, D. G. Schlom, K. J. Choi, D. M. Kim, C. B. Eom, H. P. Sun, X. Q. Pan, Y. L. Li, L. Q. Chen, Q. X. Jia, S. M. Nakhmanson, K. M. Rabe, and X. X. Xi, *Science* **313**, 1614 (2006).

¹¹E. V. Bursian and O. I. Zaikovskii, *Fiz. Tverd. Tela* **10**, 1413 (1968); E. V. Bursian and O. I. Zaikovskii, *Sov. Phys. Solid State* **10**, 1121 (1968); E. V. Bursian, O. I. Zaikovskii, and K. V. Makarov, *J. Phys. Soc. Jpn.* **28**, 416 (1970).

¹²W. Ma and L. E. Cross, *Appl. Phys. Lett.* **79**, 4420 (2001).

¹³W. Ma and L. E. Cross, *Appl. Phys. Lett.* **88**, 232902 (2006).

¹⁴Craig J. Fennie and Karin M. Rabe, *Phys. Rev. B* **72**, 100103(R) (2005).

¹⁵Nicole A. Benedek and Craig J. Fennie, *Phys. Rev. Lett.* **106**, 107204 (2011).

¹⁶L. Goncalves-Ferreira, Simon A. T. Redfern, Emilio Artacho, and Ekhard K. H. Salje, *Phys. Rev. Lett.* **101**, 097602 (2008).

¹⁷Eric Bousquet, Matthew Dawber, Nicolas Stucki, Celine Lichtensteiger, Patrick Hermet, Stefano Gariglio, Jean-Marc Triscone, and Philippe Ghosez, *Nature (London)* **452**, 732 (2008).

¹⁸V. Gopalan and D. B. Litvin, *Nature Mater.* **10**, 376 (2011).

¹⁹M. J. Haun, E. Furman, T. R. Halemane, and L. E. Cross, *Ferroelectrics* **99**, 55 (1989); **99**, 13 (1989).

²⁰A. K. Tagantsev, E. Courtens, and L. Arzel, *Phys. Rev. B* **64**, 224107 (2001).

²¹B. Houchmanzadeh, J. Lajzerowicz, and E. Salje, *J. Phys. Condens. Matter* **3**, 5163 (1991).

²²M. Daraktchiev, G. Catalan, and J. F. Scott, *Ferroelectrics* **375**, 122 (2008).

²³P. Zubko, G. Catalan, P. R. L. Welche, A. Buckley, and J. F. Scott, *Phys. Rev. Lett.* **99**, 167601 (2007).

²⁴Sandra Van Aert, Stuart Turner, Rémi Delville, Dominique Schryvers, Gustaaf Van Tendeloo, and Ekhard K. H. Salje, *Advanced Materials* **24**, 523 (2012).

²⁵M. S. Majdoub, P. Sharma, and T. Cagin, *Phys. Rev. B* **77**, 125424 (2008).

²⁶G. Catalan, B. Noheda, J. McAneney, L. J. Sinnamon, and J. M. Gregg, *Phys. Rev. B* **72**, 020102 (2005).

²⁷E. A. Eliseev, A. N. Morozovska, M. D. Glinchuk, and R. Blinc, *Phys. Rev. B* **79**, 165433 (2009).

²⁸D. Lee, A. Yoon, S. Y. Jang, J.-G. Yoon, J.-S. Chung, M. Kim, J. F. Scott, and T. W. Noh, *Phys. Rev. Lett.* **107**, 057602 (2011).

²⁹T. A. Aslanian and A. P. Levanyuk, *Pis'ma Zh. Eksp. Teor. Fiz.* **28**, 76 (1978) [*Sov. Phys. JETP Lett.* **28**, 70 (1978)].

³⁰B. Houchmanzadeh, J. Lajzerowicz, and E. Salje, *Phase Trans.* **38**, 77 (1992).

³¹P. A. Fleury and J. M. Worlock, *Phys. Rev.* **174**, 613 (1968).

³²J. F. Nye, *Physical Properties of Crystals: Their Representation by Tensors and Matrices* (Clarendon Press, Oxford, 1985).

³³A. K. Tagantsev and G. Gerra, *J. Appl. Phys.* **100**, 051607 (2006).

³⁴C. H. Woo and Yue Zheng, *Appl. Phys. A* **91**, 59 (2007).

³⁵A. M. Bratkovsky and A. P. Levanyuk, *J. Comput. Theor. Nanosci.* **6**, 465 (2009).

³⁶G. Rupprecht and R. O. Bell, *Phys. Rev.* **135**, A748 (1964).

³⁷A. N. Morozovska, E. A. Eliseev, M. D. Glinchuk, Long-Qing Chen, and Venkatraman Gopalan, Interfacial Polarization and Pyroelectricity in Antiferrodistortive Structures Induced by a Flexoelectric Effect and Rotostriction (v2), e-print [arXiv:1108.0019](https://arxiv.org/abs/1108.0019).

- ³⁸A. Y. Borisevich, O. S. Ovchinnikov, Hye Jung Chang, M. P. Oxley, Pu Yu, J. Seidel, E. A. Eliseev, A. N. Morozovska, R. Ramesh, S. J. Pennycook, and S. V. Kalinin, *ACS Nano* **4**, 6071 (2010).
- ³⁹J. Groten, M. Zirkel, G. Jakopic, A. Leitner, and B. Stadlober, *Phys. Rev. B* **82**, 054112 (2010).
- ⁴⁰A. N. Morozovska, E. A. Eliseev, S. L. Bravina, and S. V. Kalinin, *Phys. Rev. B* **75**, 174109 (2007).
- ⁴¹N. Tayebi, Y. Narui, R. J. Chen, C. P. Collier, K. P. Giapis, and Y. Zhang, *Appl. Phys. Lett.* **93**, 103112 (2008).
- ⁴²S. V. Kalinin, A. N. Morozovska, L. Q. Chen, and B. J. Rodriguez, *Rep. Prog. Phys.* **73**, 056502 (2010).
- ⁴³See Supplemental Material at <http://link.aps.org/supplemental/10.1103/PhysRevB.85.094107> for equations describing APBs, TBs, their energies and wall half-width temperature dependences.
- ⁴⁴S. B. Lang, *Phys. Today* **58**, 31 (2005).
- ⁴⁵Hiromoto Uwe and Tunetaro Sakudo, *Phys. Rev. B* **15**, 337 (1977).
- ⁴⁶N. A. Pertsev, A. K. Tagantsev, and N. Setter, *Phys. Rev. B* **61**, R825 (2000).
- ⁴⁷W. Cao and G. R. Barsch, *Phys. Rev. B* **41**, 4334 (1990).
- ⁴⁸G. A. Smolenskii, V. A. Bokov, V. A. Isupov, N. N. Krainik, R. E. Pasynkov, and A. I. Sokolov, in *Ferroelectrics and Related Materials* (Gordon and Breach, New York, 1984), p. 421.
- ⁴⁹J. Hlinka and P. Marton, *Phys. Rev. B* **74**, 104104 (2006).
- ⁵⁰R. Moos, W. Mcnesklou, and K. H. Hardtl, *Appl. Phys. A* **61**, 389 (1995).
- ⁵¹Ralf Moos and Karl Heinz Hardtl, *J. Appl. Phys.* **80**, 393 (1996).
- ⁵²Rakesh K. Behera, Chan-Woo Lee, Donghwa Lee, Anna N. Morozovska, Susan B. Sinnott, Aravind Asthagiri, Venkatraman Gopalan, and Simon R. Phillpot, *J. Phys.: Condens. Matter.* **23**, 175902 (2011).